

# Transport of Iron Oxide Colloids in Packed Quartz Sand Media: Monolayer and Multilayer Deposition

Florian Kuhnen,\* Kurt Barmettler,\* Subir Bhattacharjee,† Menachem Elimelech,† and Ruben Kretzschmar\*<sup>1</sup>

\**Institute of Terrestrial Ecology, Swiss Federal Institute of Technology Zürich, Grabenstrasse 3, CH-8952 Schlieren, Switzerland; and †Department of Chemical Engineering, Environmental Engineering Program, Yale University, New Haven, Connecticut 06520-8286*

Received December 15, 1999; accepted July 17, 2000

The transport and deposition dynamics of hematite ( $\alpha$ -Fe<sub>2</sub>O<sub>3</sub>) colloids in packed quartz sand media are investigated. Column transport experiments were carried out at various solution ionic strengths, colloid concentrations, and flow velocities. A colloid transport model was proposed that includes the dynamics of blocking as well as multilayer deposition that takes place at high ionic strengths where particle–particle interactions are favorable. Blocking dynamics in the model are described by either Langmuirian adsorption (LA) or random sequential adsorption (RSA). Two important model parameters—the particle–matrix collision efficiency and the ionic strength dependent blocking (excluded area) parameter—are estimated from the colloid breakthrough curves using a nonlinear optimization procedure. The collision (attachment) efficiency for particle–particle interactions, on the other hand, was determined independently from colloid aggregation rate measurements. At very low ionic strength, only monolayer deposition is observed and the RSA model gives a better description of the experimental data than the LA model. At higher ionic strengths, multilayer deposition becomes significant and both models yield comparable results. Calculated maximum surface coverages at low ionic strengths were in good agreement with experimentally observed values obtained by scanning electron microscopy. © 2000 Academic Press

**Key Words:** colloid transport; deposition dynamics; blocking effect; hematite; kinetics.

## INTRODUCTION

Transport of suspended colloidal particles in granular porous media is of fundamental importance in a variety of applied fields, including water and wastewater treatment, industrial separation processes, and contaminant transport in natural subsurface environments (1–3). In addition to physical factors, such as flow velocity and pore structure, the mobility of colloidal particles in porous media is largely controlled by physico-chemical interactions between the colloidal particles and between the particles and stationary matrix surfaces. The magnitude of these interactions is determined by the balance between attractive and

repulsive forces and is therefore strongly dependent on surface charge and solution chemistry (4).

A large number of studies have been conducted investigating initial colloid deposition kinetics in natural and model porous media as a function of colloid size, surface properties, flow velocity, and solution composition (5–10). In this context, the term *initial* refers to the absence of a significant amount of deposited colloidal particles on matrix surfaces. The results show that colloid deposition in porous media follows a first-order kinetic rate law and is largely irreversible at fixed chemical and physical conditions (11, 12). For model systems, filtration theory has been developed to predict the initial deposition rate of colloidal particles under favorable conditions, i.e., in the absence of repulsive forces between colloidal particles and stationary matrix surfaces (13, 14). In the presence of repulsive forces, however, the deposition rate is decreased by a factor  $\alpha$  ( $0 < \alpha < 1$ ), which is often termed the collision (or attachment) efficiency. In the presence of attractive electrostatic forces, the deposition rate can also be slightly enhanced ( $\alpha > 1$ ) at very low ionic strengths (15). Attempts to predict the attachment efficiency as a function of surface charge and ionic strength based on the well-known DLVO theory have not yet been satisfactory, tending to underestimate deposition rates in the slow regime ( $\alpha < 1$ ) by several orders of magnitude (5, 16). This discrepancy between experimental data and theory has at least in part been attributed to surface charge heterogeneity of colloid and matrix surfaces, which appears to be important even in well-defined model systems (17).

In many practical situations, a continuous inflow of colloidal particles into a porous medium can occur. In such situations, as matrix surfaces are increasingly covered by deposited colloidal particles, the colloid deposition rate can either increase, remain constant, or decrease with time (12, 18–20). A decrease in colloid deposition rate, associated with the so-called *blocking effect*, is observed when the colloidal particles are stable so that repulsive particle–particle interactions predominate. In this case, only a monolayer of deposited particles is formed, and the maximum fractional surface coverage depends on the ionic strength of the solution because of lateral electrostatic repulsion between colloidal particles near the matrix surface. Constant or increased colloid deposition rates with time are commonly observed when the colloidal particles are unstable; i.e., particle–particle

<sup>1</sup> To whom correspondence should be addressed. E-mail: [kretzschmar@ito.umnw.ethz.ch](mailto:kretzschmar@ito.umnw.ethz.ch).

interactions occur and lead to the formation of multilayers of deposited particles on matrix surfaces. Both effects have been observed experimentally in model systems (19, 21, 22) as well as natural subsurface porous media (12).

Models have recently been proposed to describe blocking effects in ideal model systems where repulsive electrostatic interparticle forces predominate and multilayer deposition is not feasible (18, 20, 23). Under these conditions where blocking and monolayer deposition prevail, experimental results are usually in good agreement with model predictions (18, 20–22). However, studies on the dynamics of colloid deposition under conditions where multilayer deposition occurs are scarce (8, 21, 22, 24). These models of multilayer deposition often consider a simple Langmuirian blocking behavior to account for the coverage of the bare collector surfaces by the deposited particles (21, 24). Studies on monolayer deposition in granular porous media, however, strongly indicate that random sequential adsorption (RSA) blocking dynamics (18, 23) portrays the colloid deposition behavior at higher surface coverages more accurately. Furthermore, the RSA blocking dynamics is fundamentally related to the electrostatic and hydrodynamic forces governing the porous medium (8, 23) and, hence, is capable of relating the colloid deposition behavior to the physico-chemical conditions in a given system. Although the above features render this model superior to the Langmuirian blocking model, the influence of RSA blocking dynamics on multilayer deposition of colloidal particles has not been assessed so far.

The aim of the present study was to investigate the dynamics of colloid deposition as a function of ionic strength, flow rate, and particle concentration using a model system consisting of quartz grains as the porous medium and hematite ( $\alpha$ - $\text{Fe}_2\text{O}_3$ ) particles as mobile colloids. A transport model is developed that accounts for hydrodynamic dispersion, blocking effects, and multilayer deposition of hematite particles on surfaces of quartz grains. Two different blocking functions, namely, Langmuirian (LA) and random sequential adsorption (RSA), were used and compared for their ability to describe the experimental data. In addition, the maximum surface coverage at low ionic strength was determined by direct counting and was compared with model calculations. The hematite–quartz system was chosen because it is environmentally relevant but yet sufficiently well defined to allow a quantitative analysis of the data. Iron oxide colloids are common in subsurface aquatic environments and can potentially serve as carriers for groundwater pollutants (25–27).

## EXPERIMENTAL

### *Colloidal Hematite Particles*

Submicrometer-sized hematite particles were synthesized by aging a concentrated iron hydroxide gel (28). The gel was prepared by adding 100 ml of 6 M NaOH (Merck, p.a.) to 100 ml of 2 M  $\text{FeCl}_3$  (Fluka, p.a.) in a Pyrex glass bottle and mixing with a propeller stirrer for 10 min. The bottle was tightly capped and placed in an oven set to 100°C for aging. After 72 h, the

sample was cooled to room temperature. Excess salts were removed by washing the particles twice with deionized water by centrifugation and then dialyzing the suspension against deionized water for 12 days. The resulting stock suspension was stored in a polyethylene bottle in the dark at 4°C.

The hematite suspension was characterized by transmission electron microscopy, X-ray diffraction analysis, acid–base titrations, electrophoretic mobility measurements, and  $\text{N}_2$ -BET surface area analysis (29). The hematite particles were of spheroidal shape and rather uniform in size, with an average diameter of  $122 \pm 29$  nm (800 particles measured by TEM). The specific surface area of the particles was 27  $\text{m}^2/\text{g}$ , according to the  $\text{N}_2$ -BET method (30). Acid–base titration experiments and electrophoretic mobility measurements showed that the particles had a point of zero charge (PZC) at pH 9.3, which is in excellent agreement with theoretical considerations for the hematite surface (31). Mineral impurities were not detected in the sample.

### *Column Transport Experiments*

Colloid deposition dynamics was investigated by conducting a series of column transport experiments at different ionic strengths, colloid concentrations, and flow velocities. Glass chromatography columns (Omnifit, Cambridge, England) with 1-cm inner diameter and 3-cm length were uniformly packed with quartz sand (Aldrich Chemical, Milwaukee, WI). Before use, the sand was thoroughly cleaned by washing with sodium dithionite (0.1 M  $\text{Na}_2\text{S}_2\text{O}_4$ ) and hydrogen peroxide (5%  $\text{H}_2\text{O}_2$ ) solutions, followed by washing with concentrated hydrochloric acid (12 M HCl) and deionized water. The sand grains were rather uniform in size and had an average diameter of about 300  $\mu\text{m}$ .

The experimental setup used for the transport experiments is illustrated in Fig. 1. The sand columns were first flushed with  $\text{CO}_2$  gas to replace the air and were then water saturated by passing a  $\text{NaNO}_3$  solution (0–100 mM; pH 5.8) through the column in the upward direction at a rate of 1.3 ml/min. The flow rate of the solution was controlled by an HPLC pump (Jasco, Japan). The columns were then connected to an additional peristaltic pump (Ismatec, Switzerland; with Masterflex Quick-Load Head) delivering a well-dispersed hematite suspension (111 mg/L; pH 5.8). To minimize particle aggregation at higher ionic strengths, the two feed solutions were mixed at a volume ratio of 1 : 1 shortly before the column inlet, resulting in an inflow hematite particle concentration of approximately 55 mg/L. This particle concentration corresponded to approximately  $10^{16}$  particles/L (Table 1). At the column outlet, a 0.1 g/L hexametaphosphate (HMP) solution was added to the column effluent to stabilize the colloidal particles using a second HPLC pump set to 0.25 ml/min. HMP strongly adsorbs to the hematite surface and causes charge reversal from positive to negative, which prevented colloid attachment to walls of tubings and vials and also prevented particle aggregation prior to determination of particle concentration. The stabilized effluent suspension was collected in regular time intervals using an automated fraction

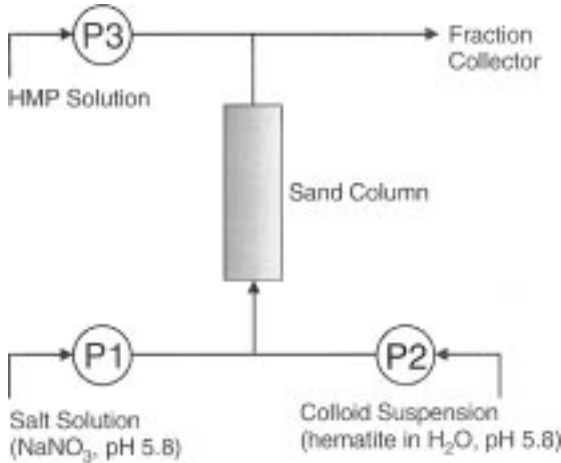


**FIG. 1.** Schematic drawing of the experimental setup used for colloid transport experiments. A 1 : 1 electrolyte solution ( $\text{NaNO}_3$ ) was pumped through the sand column using HPLC pump P1. Colloidal hematite particles were added to the inflow solution shortly before entering the column using peristaltic pump P2. At the column outlet, a dilute hexametaphosphate (HMP) solution was added using HPLC pump P3 to stabilize the colloidal particles in suspension. The effluent suspension was collected with a fraction collector and analyzed for particle concentration.

collector and analyzed for colloid concentration by light absorbance at 430 nm. A series of standard hematite suspensions was used for calibration. All transport experiments were carried out at pH 5.8 and 25°C.

The sand columns were characterized by saturating them with 0.1 M NaCl solution and injecting a 0.1-ml pulse of 0.001 M  $\text{NaNO}_3$  solution. The nitrate concentration in the effluent was monitored using an on-line UV-VIS detector set to a wavelength of 220 nm. The first and second moments of the nitrate breakthrough curves were analyzed numerically to determine the column pore volume and dispersivity, respectively (32). In the model calculations, a theoretical dispersivity value was used, as explained below. This theoretical value was in good agreement with experimental values resulting from tracer pulse experiments.

**TABLE 1**

**Experimental Parameters for the Colloid Transport Experiments (Measured Values)**

Experiment number	Flow velocity [ $10^{-4}$ m/s]	Colloid concentration [ $10^{16}$ particles/L]	$\text{NaNO}_3$ concentration [mM]
1	2.38	1.21	<0.01
2	2.08	1.07	0.10
3	2.12	1.14	3.06
4	2.46	1.25	9.43
5	2.11	1.09	31.00
6	2.06	1.06	105.00
7	1.06	1.11	0.10
8	4.23	1.07	0.10
9	2.08	0.27	0.10

## Scanning Electron Microscopy

After completion of the colloid transport experiments, the sand was carefully removed from the columns and placed in ultrafiltered, deionized water. The water was exchanged several times with acetone. Single sand grains were air dried, mounted on sample holders for scanning electron microscopy (SEM), and sputter-coated with 5-nm platinum. The samples were viewed on a high-resolution SEM (Hitachi S-900 field emission scanning electron microscope) set to 20-keV accelerating voltage and secondary or backscattered electron imaging modes. The surface coverage with colloidal particles was determined by counting the hematite particles on a total quartz grain surface area of 288  $\mu\text{m}^2$ .

## MATHEMATICAL MODELING

### The Colloid Transport and Deposition Dynamics Equation

Under steady-state saturated flow conditions, the evolution of the suspended particle concentration  $C(x, t)$  as a function of travel distance  $x$  and time  $t$  can be described by an advection–dispersion transport equation including a term to account for the deposition of colloidal particles to stationary matrix surfaces (3, 18):

$$\frac{\partial C}{\partial t} = D_h \frac{\partial^2 C}{\partial x^2} - v_p \frac{\partial C}{\partial x} - f \frac{\partial C_s}{\partial t}. \quad [1]$$

Here,  $D_h$  is the hydrodynamic dispersion coefficient for colloidal particles,  $v_p$  is the average interstitial velocity of colloidal particles, and  $f$  is the bare matrix surface area available for colloid deposition per unit pore volume.

In our model, the surface concentration of deposited particles  $C_s(x, t)$  is given by

$$\frac{\partial C_s}{\partial t} = [k_{pc}B(\theta) + k_{pp}\theta]C, \quad [2]$$

where  $k_{pc}$  is the deposition rate of colloidal particles to bare matrix surfaces,  $k_{pp}$  is the deposition rate of colloidal particles to previously deposited particles attached to matrix surfaces,  $\theta$  is the fraction of the bare surface covered with colloidal particles, and  $B(\theta)$  is a so-called dynamic blocking function. The last term in Eq. [2] accounts for the multilayer deposition of the particles and does not incorporate any additional blocking (or ripening) mechanism since it is assumed that the rate of particle–particle deposition,  $k_{pp}$ , is independent of the thickness of the multilayers formed. Thus, possible increases in the overall deposition rate with time due to an increase in the effective surface area available for colloid capture cannot be described by the model. It should be noted, however, that the model may be extended to account for such effects by including a parameter mathematically analogous to the dynamic blocking function in the last term of Eq. [2].

Equations [1] and [2] can be combined, yielding

$$\frac{\partial C}{\partial t} = D_h \frac{\partial^2 C}{\partial x^2} - v_p \frac{\partial C}{\partial x} - f[k_{pc}B(\theta) + k_{pp}\theta]C. \quad [3]$$

The dispersion coefficient  $D_h$  was calculated from the relationship (33)

$$D_h = D_\infty/\tau + \alpha_L v_p, \quad [4]$$

where  $D_\infty$  is the Stokes–Einstein particle diffusion coefficient,  $\tau$  is the tortuosity of the medium, and  $\alpha_L$  is the dispersivity parameter. The dispersivity parameter was obtained from tracer experiments performed using quartz sand grains in columns identical to those used in the present study, and the value of the parameter was  $7 \times 10^{-4}$  m.

### Boundary and Initial Conditions

The governing differential equation for the coupled colloid transport and deposition model, Eq. [3], can be solved numerically for a given set of operating conditions to yield the colloid breakthrough curves, which represent the evolution of the effluent colloid concentration (scaled with respect to the feed concentration) with time. The boundary conditions at the column entrance and exit used in conjunction with the above transport model are, respectively (18, 19, 24),

$$C = C_0 \quad \text{at } t > 0 \text{ and } x = 0 \quad [5a]$$

$$\frac{\partial C}{\partial x} = 0 \quad \text{at } x = L \text{ for all } t, \quad [5b]$$

where  $L$  represents the column length and  $C_0$  is the colloid concentration in the column influent. Finally, the initial conditions for the problem are

$$C = 0 \quad \text{for } 0 \leq x \leq L \text{ and } t \leq 0 \quad [6a]$$

and

$$\theta = 0 \quad \text{for } 0 \leq x \leq L \text{ and } t \leq 0, \quad [6b]$$

where the statement in Eq. [6b] defines the initial condition for Eq. [2].

Solution of the transport and deposition equation [3] provides the particle breakthrough curves as well as the complete time evolution of the fractional surface coverage. The appropriately nondimensionalized governing transport equations were solved numerically using the method of lines coupled with a backward difference scheme for the time integration (34, 35). The model, as outlined above, still requires an independent mathematical expression for the dynamic blocking function,  $B(\theta)$ , and the pertinent formulations for this function are presented next.

### Dynamic Blocking Functions

Different expressions have been proposed for the dynamic blocking function  $B(\theta)$ , two of which will be compared in this

paper. The first is based on the Langmuirian adsorption (LA) model with

$$B(\theta) = 1 - \beta\theta. \quad [7]$$

The second is based on the random sequential adsorption (RSA) model (18, 23)

$$B(\theta) = 1 - 4\beta\theta + \frac{6\sqrt{3}}{\pi}(\beta\theta)^2 + \left(\frac{40}{\sqrt{3}\pi} - \frac{176}{3\pi^2}\right)(\beta\theta)^3, \quad [8]$$

where the cubic polynomial expression is valid up to a fractional coverage of ca. 0.4 (23). The parameter  $\beta$  is defined as the inverse of the maximum fractional surface coverage ( $\beta = 1/\theta_{\max}$ ). Noting that Eqs. [7] and [8] are modifications of the hard-sphere blocking behavior (in which case,  $\beta = 1$ ) to account for the electrostatic repulsion between the deposited particles, the blocking (or excluded area) parameter  $\beta$  reflects the deviation of the maximum surface coverage from the hard-sphere jamming limits due to electrostatic forces. Because of lateral electrostatic repulsive interactions between particles near the matrix surface, the blocking parameter  $\beta$  is expected to increase with decreasing ionic strength (18, 36). It is important to note that in light of the different maximum allowable surface coverages in the Langmuir ( $\theta_{\max}^{\text{LA}} = 1$ ) and the hard-sphere RSA ( $\theta_{\max}^{\text{RSA}} = 0.546$ ) models (18, 21, 23), the parameter  $\beta$  should be interpreted differently when using Eqs. [7] and [8]. Further differences in the interpretation of  $\beta$  in the LA and RSA models are pointed out in the Results and Discussion section (18, 36).

### Model Parameters

In both models, the change in surface coverage  $\theta$  with time can be expressed as

$$\frac{\partial \theta}{\partial t} = k_{pc}B(\theta)\pi\alpha_p^2 C. \quad [9]$$

The overall colloid deposition rate constants  $k_{pc}$  and  $k_{pp}$  in granular porous media can be interpreted as the product of the fast deposition rate under favorable conditions  $k^f$  (in the absence of electrostatic repulsive or attractive forces) and a collision efficiency for particle–matrix and particle–particle interactions, respectively,

$$k_{pc} = k^f \alpha_{pc} \quad [10]$$

and

$$k_{pp} = k^f \alpha_{pp}. \quad [11]$$

The initial deposition rate under favorable conditions,  $k^f$ , can be calculated from filtration theory (4, 13).

The blocking and multilayer deposition model described above is schematically illustrated in Fig. 2. At low ionic strength, the collision efficiency for particle–particle interactions,  $\alpha_{pp}$ , is

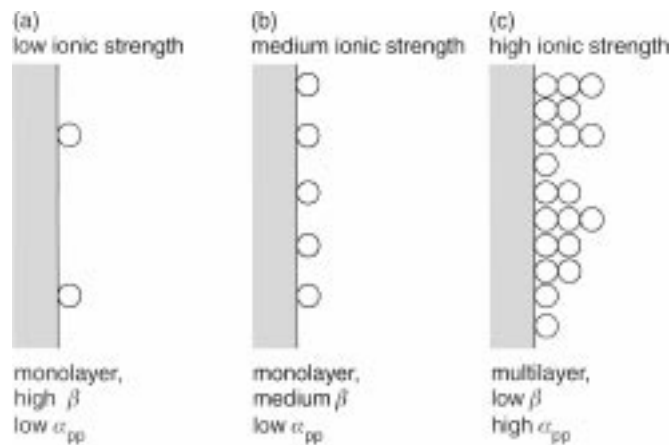


**FIG. 2.** Illustration of the colloid deposition model with blocking effect and multilayer deposition. (a) At low ionic strength, low particle-particle collision efficiency  $\alpha_{pp}$  and high blocking parameter  $\beta$  lead to the development of a thin monolayer. (b) At medium ionic strength, low particle-particle collision efficiency  $\alpha_{pp}$  and decreased blocking parameter  $\beta$  lead to a denser monolayer coverage. (c) At high ionic strength, high particle-particle collision efficiency  $\alpha_{pp}$  and low blocking parameter  $\beta$  lead to multilayer deposition.

very low and the blocking parameter  $\beta$  is high, resulting in a sparse monolayer at maximum coverage. With increasing ionic strength the  $\beta$  parameter increases, resulting in a denser monolayer coverage. Further increases in ionic strength lead to increased  $\alpha_{pp}$  and hence result in multilayer deposition, described in this model by stacking of particles in a string-like fashion.

For a given set of hydrodynamic and physico-chemical conditions, the present model can be used to determine the breakthrough behavior, provided three parameters, namely, the collision efficiencies ( $\alpha_{pc}$  and  $\alpha_{pp}$ ) and the blocking parameter ( $\beta$ ) are known independently. The collision efficiencies for particle-matrix and particle-particle interactions and the blocking parameter strongly depend on the surface charge of the colloids and matrix surfaces and on the ionic composition of the medium. In this study, the collision efficiency for particle-matrix collisions,  $\alpha_{pc}$ , and the blocking parameter,  $\beta$ , were estimated by reconciling the experimental breakthrough data and the deposition model described above using a nonlinear optimization procedure. The Levenberg-Marquardt method (37) was used to estimate the two deposition parameters by minimizing the sum-squared errors between the experimental and theoretical particle breakthrough profiles. The collision efficiency for particle-particle collisions of hematite colloids was determined independently from aggregation rate measurements in dilute suspensions using dynamic light scattering (29).

## RESULTS AND DISCUSSION

### Influence of Ionic Strength on Colloid Transport

The results of the colloid transport experiments conducted at different ionic strengths (Experiments 1–7, Table 1) are presented as breakthrough curves in Fig. 3a. In all experiments, the

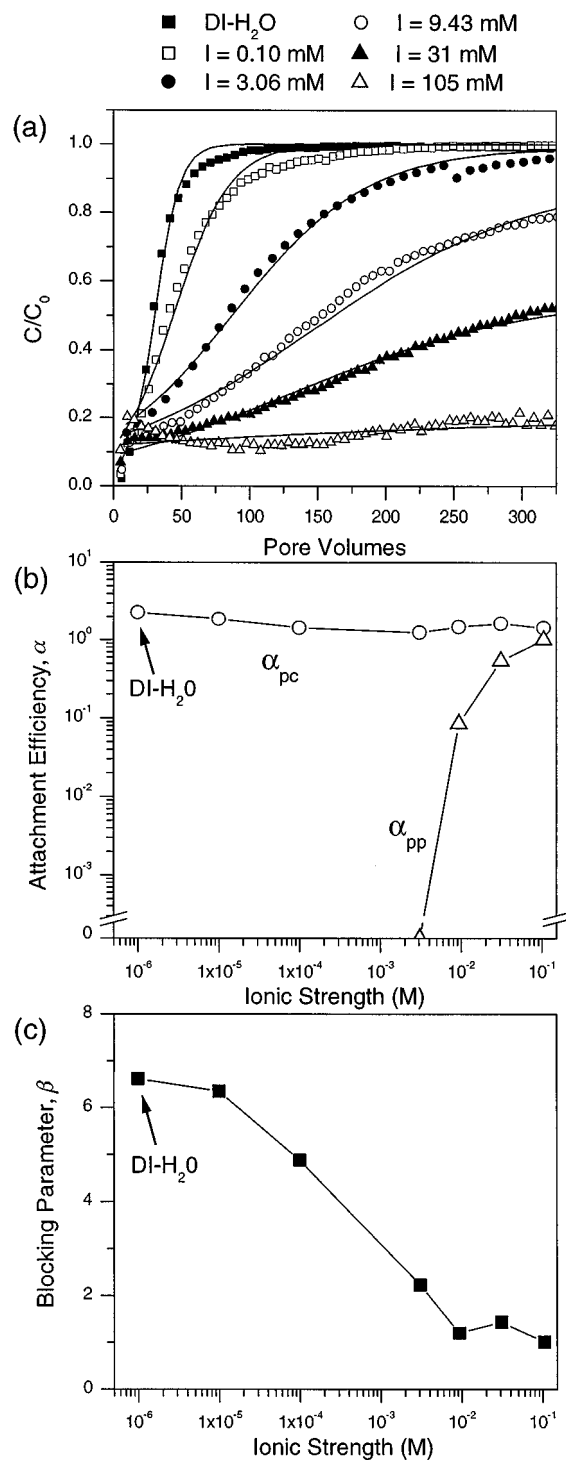


**FIG. 3.** (a) Breakthrough curves of hematite colloids through columns packed with quartz sand at different ionic strengths. Lines represent model calculations based on estimated parameters obtained with the Langmuirian blocking function and multilayer deposition. (b) Collision efficiencies for particle-matrix interactions,  $\alpha_{pc}$ , and particle-particle interactions,  $\alpha_{pp}$ , as a function of ionic strength of the solution. (c) Blocking parameter,  $\beta$ , as a function of ionic strength in solution. The two parameters  $\alpha_{pc}$  and  $\beta$  were fitting parameters, whereas  $\alpha_{pp}$  was determined independently.

relative colloid concentration in the effluent  $C/C_0$  increased to values around 0.15 after the first pore volume. This initial colloid breakthrough depends on the *initial* deposition rate of colloidal particles on the clean quartz grains. Since the hematite colloids and quartz grains possess opposite surface charge, fast deposition kinetics is expected ( $\alpha_{pc} \approx 1$ ). At very low ionic strengths ( $<10^{-4}$  M), the deposition rate may be even slightly accelerated ( $\alpha_{pc} > 1$ ) due to the enhanced long-range electrostatic attraction between positively charged hematite colloids and negatively charged quartz surfaces. Further evolution of the colloid concentration with time was strongly ionic strength dependent. At the lowest ionic strength (DI- $H_2O$ ), the colloid concentration increased rapidly and reached  $C/C_0 = 1$  after about 100 pore volumes. This breakthrough behavior indicates that the maximum surface coverage is rather low and that multilayer deposition is negligible, due to electrostatic repulsion between the colloidal particles at low ionic strength. When the ionic strength was increased to 0.1 or 3 mM  $NaNO_3$ , the colloid concentrations in the effluent also reached  $C/C_0 = 1$ , but much more gradually. Thus, multilayer deposition was still negligible, but the maximum surface coverage was increased due to increased screening of particle surface charge. When the ionic strength was further increased, multilayer deposition became important and the effluent concentrations leveled off at  $C/C_0 < 1$ , depending on the rate of particle–particle interactions.

The lines in Fig. 3a represent the best fit descriptions of the experimental breakthrough curves with the model based on the Langmuirian blocking function and multilayer deposition (Eqs. [3] and [7]). In the model breakthrough curves, the estimated collision efficiency for particle–matrix interactions,  $\alpha_{pc}$ , and blocking parameter,  $\beta$ , were used. As mentioned earlier, the collision efficiency for particle–particle interactions,  $\alpha_{pp}$ , was determined independently by dynamic light scattering experiments in dilute suspensions (29). Overall, the model describes the features of the colloid breakthrough curves at different ionic strengths rather well, although small deviations still remain. At the lowest two ionic strengths, where the blocking effect is dominant, the model does not accurately describe the change in deposition rate at high surface coverages, i.e., near  $\theta_{max}$ . At the highest ionic strength, where multilayer deposition is dominant, small deviations from the experimental data also occur.

Figures 3b and 3c show the three model parameters,  $\alpha_{pc}$ ,  $\alpha_{pp}$ , and  $\beta$ , as a function of solution ionic strength. The particle–matrix collision efficiency is always expected to be unity, with a slight increase at very low ionic strength ( $<10^{-4}$  M), because of electrostatic attraction between positively charged hematite colloids and negatively charged quartz surfaces. As evident in Fig. 3b, the fitted value for  $\alpha_{pc}$  was only slightly greater than unity, and it indeed exhibited a slight increase at very low ionic strength. Since filtration theory was used to calculate the rate of fast deposition, based on the assumption of a packed bed of uniform and smooth spherical collector grains, deviations from the expected value are most likely due to surface roughness and nonideal shapes of the quartz grains. The  $\alpha_{pp}$  values shown in

Fig. 3b are strongly ionic strength dependent, as expected from DLVO theory. At low ionic strength, the particles are very stable due to electrostatic repulsion between the positively charged hematite colloids. With increasing ionic strength, the surface charge is increasingly screened, resulting in increased collision efficiencies for aggregation or multilayer deposition,  $\alpha_{pp}$ . At very high ionic strength, the collision efficiency reaches a value of unity, as would be expected from DLVO theory. The blocking parameter  $\beta$  is near unity at high ionic strength and increases with decreasing ionic strength, implying that at low ionic strength a single deposited particle is blocking a larger surface area than that at higher ionic strength. Thus, the dependence of the blocking parameter on electrolyte concentration is in conformity with theoretical expectations.

The model calculations and the estimated model parameters based on random sequential adsorption (RSA) and multilayer deposition are depicted in Fig. 4. This model was clearly more accurate in describing the development of colloid concentrations with time at low ionic strength, where the blocking effect is dominant. The better performance of the RSA blocking function over the Langmuirian blocking function is most pronounced at intermediate to high surface coverage relative to the maximum surface coverage, that is, in the later stages of colloid deposition. At higher ionic strength, where multilayer deposition occurs, small deviations between the experimental data and the model calculations remain. These deviations may be related to the simplifying assumption that multilayers build up only in a chain-like fashion on top of colloidal particles attached to the quartz surfaces (Fig. 2). The model parameters again behave as expected, with  $\alpha_{pc}$  close to unity and largely independent of ionic strength,  $\alpha_{pp}$  strongly ionic strength dependent, and  $\beta$  increasing with decreasing ionic strength.

At this juncture, one should note that the values of the blocking parameter  $\beta$  obtained using the LA and RSA models (Figs. 3c and 4c) differ by a (nearly) constant factor of 0.44 ( $\beta_{RSA} \approx 0.44\beta_{LA}$ ). This difference stems from the different definitions of the blocking parameter embedded in the two blocking models. From Eqs. [7] and [8], it can be seen that the dynamic blocking function  $B(\theta)$  becomes zero when  $\beta\theta = 1$  for the LA model and when  $\beta\theta = 0.44^2$  (the real root of the cubic equation) for the RSA model, respectively. Thus, for a given surface coverage,  $\theta$ , the parameter  $\beta$  predicted by the RSA model will be approximately 0.44 times the corresponding prediction based on the LA model.

#### Maximum Surface Coverage at Low Ionic Strength

The transition from monolayer to multilayer deposition with increasing ionic strength was also studied by examining single sand grains taken from the columns at the end of the transport

<sup>2</sup> This value differs from the jamming limit of the hard-sphere RSA model (0.546), owing to our use of the low to moderate coverage virial form of the dynamic blocking function in Eq. [8].

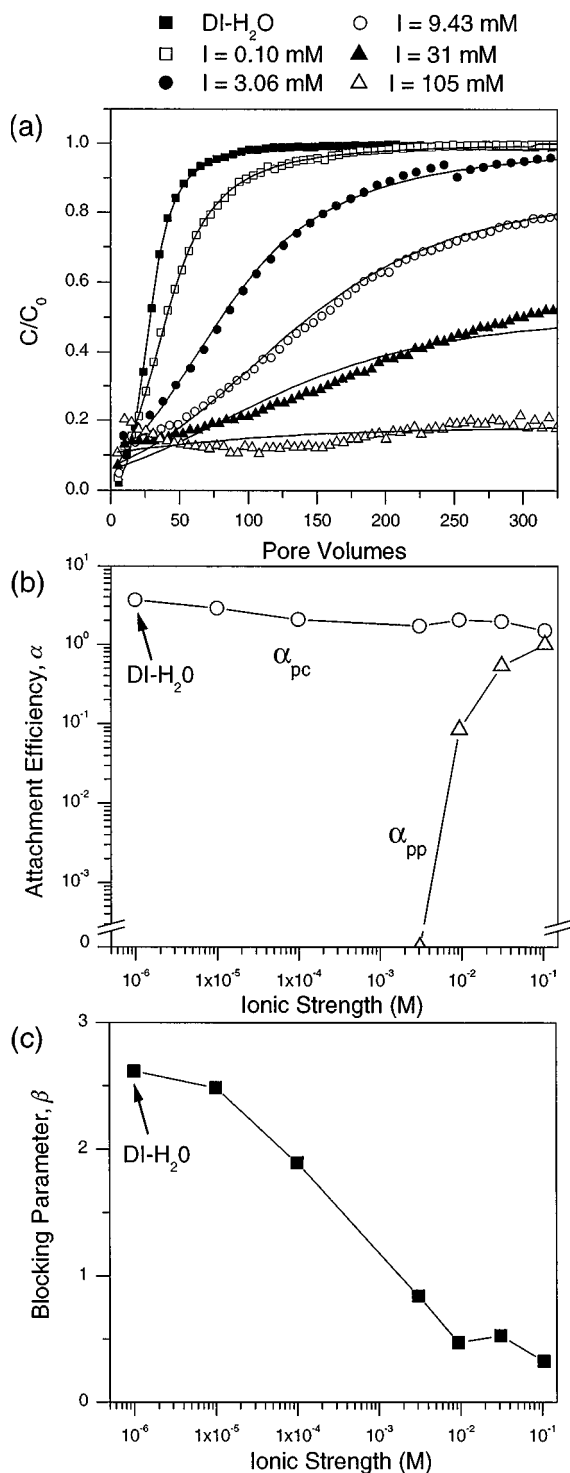


**FIG. 4.** (a) Breakthrough curves of hematite colloids through columns packed with quartz sand at different ionic strengths. Lines represent model calculations based on estimated parameters obtained with the random sequential adsorption blocking function and multilayer deposition. (b) Collision efficiencies for particle–matrix interactions,  $\alpha_{pc}$ , and particle–particle interactions,  $\alpha_{pp}$ , as a function of ionic strength of the solution. (c) Blocking parameter,  $\beta$ , as a function of ionic strength in solution. The two parameters  $\alpha_{pc}$  and  $\beta$  were fitting parameters, whereas  $\alpha_{pp}$  was determined independently.

experiments by scanning electron microscopy. Figure 5a shows a typical sand grain, illustrating that the grains are nonspherical and exhibit significant surface roughness. Figures 5b, 5c, and 5d show backscattered SEM images of representative areas on sand grains from the experiments conducted with hematite suspended in DI-H<sub>2</sub>O, 0.1 mM NaNO<sub>3</sub>, and 3 mM NaNO<sub>3</sub>, respectively. At very low ionic strength, only a monolayer of single hematite particles was observed on the surfaces of quartz grains (Figs. 5b and 5c). The density of particles on the surface increased with increasing ionic strength, in accordance with the decrease in  $\beta$  with increasing ionic strength. At higher ionic strength, clear multilayer deposition was observed, due to attachment of suspended hematite particles to previously deposited hematite particles on the surface. Thus, these results are in qualitative agreement with the model parameters given in Figs. 3 and 4.

For the two lowermost ionic strengths, where only monolayers of hematite particles were formed and complete particle breakthrough ( $C/C_0 = 1$ ) was reached at the end of the experiments, an attempt was made to experimentally quantify the maximum surface coverage by counting the attached particles on scanning electron micrographs. The results are given in Table 2 and are compared with the calculated maximum surface coverages resulting from mass balance calculations and LA- and RSA-based model parameter estimation. In the mass balance calculations, the amount of attached particles at maximum surface coverage was estimated from the area above the breakthrough curve, taking  $C/C_0 = 1$  as the upper boundary and correcting for the first pore volume (19). The maximum surface coverage for the two ionic strengths obtained by SEM was in good agreement with the values resulting from model calculations and mass balance, with a slight tendency of yielding lower values. Again, this deviation may be explained by a higher surface area of the quartz sand than that assumed in the model calculations, due to polydispersity and nonspherical shape of the sand grains (Fig. 5a). In the model calculations, the surface area of the quartz sand was estimated from the average grain size assuming spherical shape.

#### Effects of Particle Concentration and Flow Velocity

Three additional transport experiments were conducted to test the ability of the models to predict the colloid breakthrough curves at different influent particle concentrations and flow

**TABLE 2**  
Maximum Surface Coverage at Low Ionic Strength Measured by Direct Counting on Scanning Electron Micrographs (SEM), Mass Balance Calculations, and Fitting of the Langmuirian- (LA-) and Random Sequential Adsorption- (RSA-) Based Transport Models

Ionic strength [M]	Maximum surface coverage, $\theta_{max}$			
	SEM <sup>a</sup>	Mass balance	LA fit	RSA fit
$<10^{-5}$	$0.10 \pm 0.01$	0.15	0.15	0.17
$10^{-4}$	$0.19 \pm 0.02$	0.21	0.21	0.23

<sup>a</sup> The total analyzed surface area for each sample was  $288 \mu\text{m}^2$ .

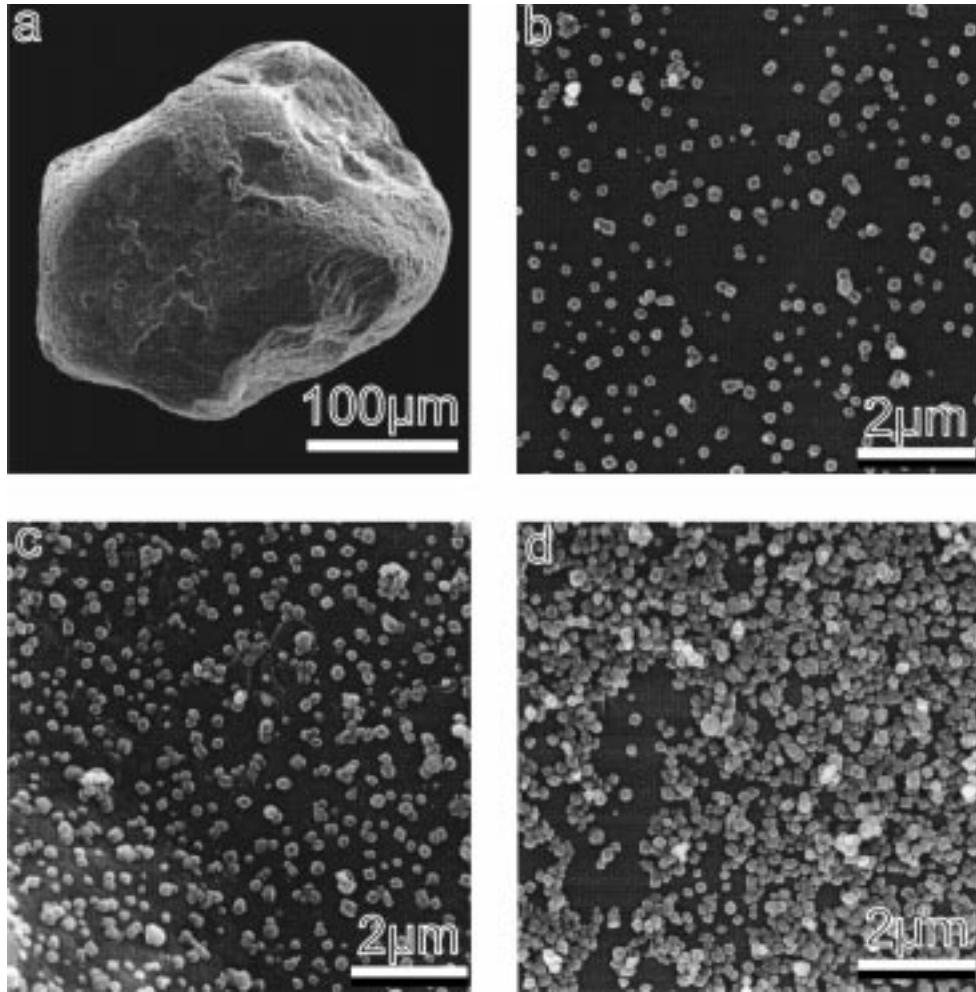


**FIG. 5.** Scanning electron microscopy images of a typical quartz grain (a) and hematite particles deposited on the quartz surface at the end of transport experiments conducted at different ionic strengths: (b)  $<10^{-5}$  M (DI-H<sub>2</sub>O), (c) 0.1 mM NaNO<sub>3</sub>, and (d) 31 mM NaNO<sub>3</sub>.

velocities. The experimental results along with model predictions using the LA-based model are presented in Fig. 6. Similar predictions were also obtained with the RSA-based transport model (Fig. 7). The experimental breakthrough curves shown with open circles were used to estimate the three deposition parameters  $\alpha_{pc}$ ,  $\alpha_{pp}$ , and  $\beta$ . Assuming that these parameters, particularly  $\beta$ , depend predominantly on the ionic strength, and do not vary appreciably over the range of particle concentrations or approach velocities used in the study, the breakthrough curves shown with solid symbols were predicted using these parameters. As evident in Figs. 6a and 7a, both LA and RSA model predictions (lines) correctly accounted for the experimental dependence of the breakthrough behavior on changes in the feed colloid concentration. When the particle concentration is decreased, it takes a much longer time to reach the maximum surface coverage and to decrease the overall deposition rate to zero (i.e.,  $C/C_0 = 1$ ).

The influence of the flow velocity on the breakthrough behavior is shown in Figs. 6b and 7b. It is evident that the

predicted breakthrough curves (lines) based on the LA and RSA models also correctly account for the influence of flow velocity on the deposition behavior. Increasing flow velocity results in a greater initial colloid breakthrough after one pore volume and a faster blocking of quartz surfaces thereafter while decreasing the flow velocity has the opposite effect. It should be kept in mind, however, that the coefficients of the RSA blocking function, Eq. [8], are susceptible to modification due to the hydrodynamic interactions (18, 38) and, consequently, should depend on the approach velocity. This implies that the blocking parameter  $\beta$  should depend on the approach velocity, which was not considered in the predicted breakthrough curves. The slight deviations between the predicted and experimental breakthrough curves in Fig. 7b might be attributed to such a phenomenon. However, this point was not pursued further since the small discrepancies may also arise due to several other competing factors, including the assumptions in the model and irregularities in the collector geometry.

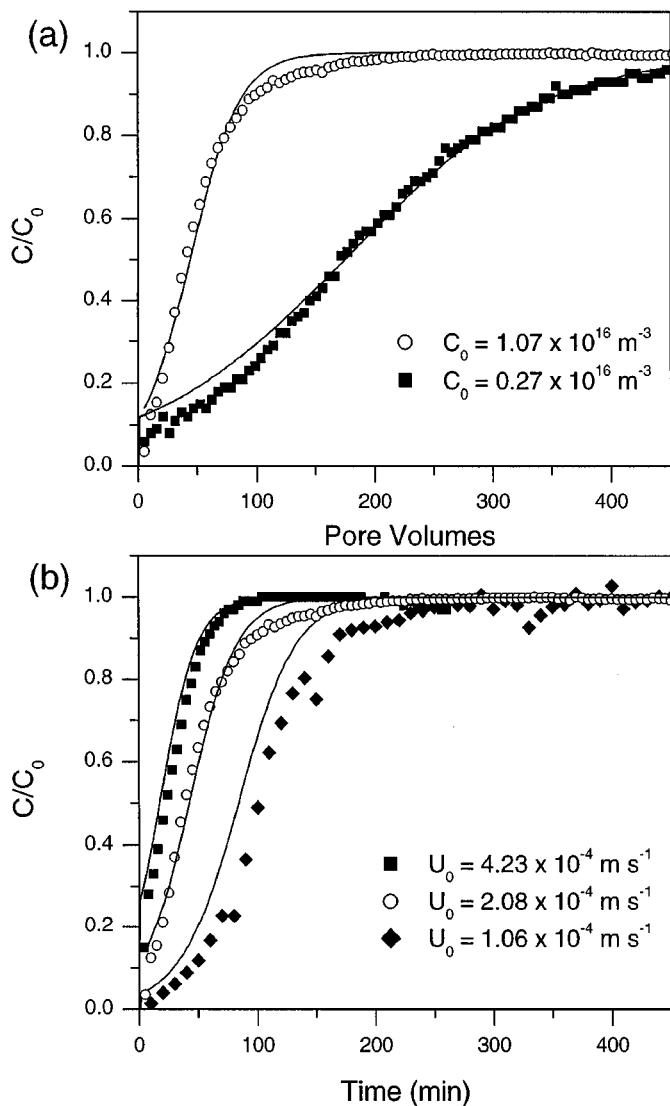


**FIG. 6.** Breakthrough curves of hematite colloids through columns packed with quartz sand at (a) different initial particle concentrations and (b) different flow velocities. The experimental breakthrough curve plotted with open circles was used to estimate the particle–matrix collision efficiency  $\alpha_{pc}$  and the blocking parameter  $\beta$  at  $10^{-4}$  M ionic strength based on the Langmuirian blocking function. The experiments shown with solid symbols were predicted using the same model parameters.

### CONCLUDING REMARKS

The results of this study demonstrate that, in the case of opposite charge of colloid and collector surfaces, the ionic strength dependent colloid transport behavior in granular porous media can be described quite accurately by a model accounting for blocking effects at low ionic strength and additional multilayer deposition at moderately high ionic strengths. Two different dynamic blocking functions were compared, the Langmuirian (LA) model and the random sequential adsorption (RSA) model. The results at low ionic strengths indicate that the RSA model more accurately describes the dynamics of colloid deposition under

the influence of surface blocking by attached colloidal particles. Both models were able to correctly predict the influence of flow velocity and initial particle concentration on the colloid breakthrough curves. Maximum surface coverages calculated by the models were in good agreement with values determined by direct particle counting of SEM images. Although both the LA and RSA models appear to predict the breakthrough behavior reasonably well, a closer inspection of the theoretical predictions suggests that the RSA model provides a better explanation of the particle deposition behavior at higher surface coverages. This result is particularly encouraging in light of the fact that the present theoretical approach employs the same number of

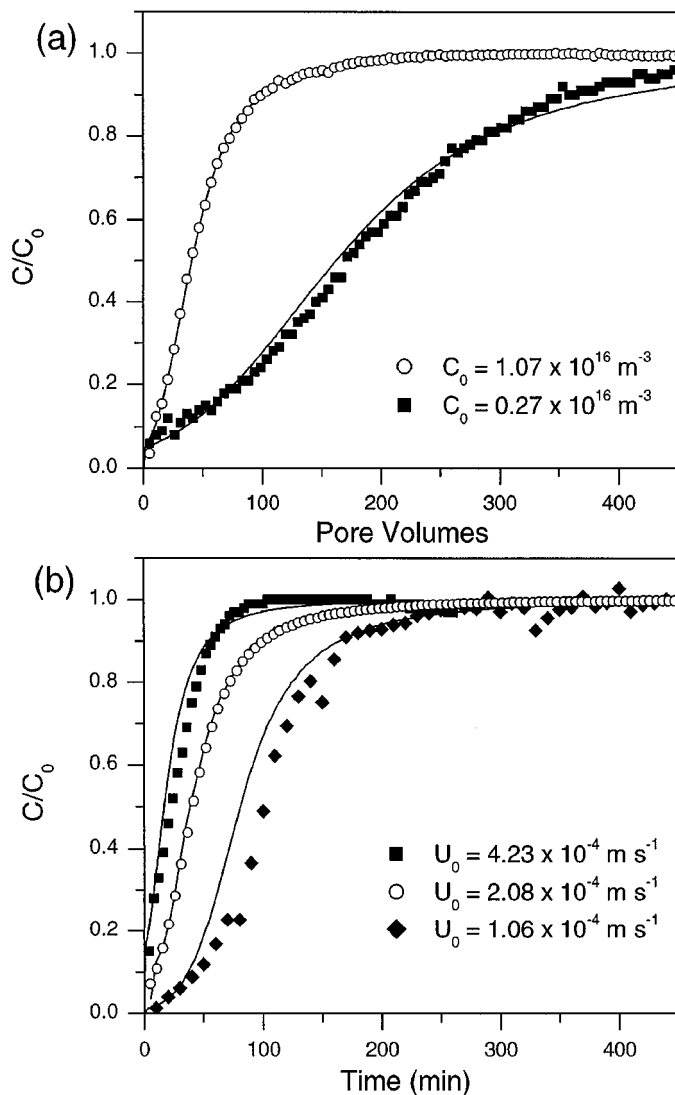


**FIG. 7.** Breakthrough curves of hematite colloids through columns packed with quartz sand at (a) different initial particle concentrations and (b) different flow velocities. The experimental breakthrough curve plotted with open circles was used to estimate the particle–matrix collision efficiency  $\alpha_{pc}$  and the blocking parameter  $\beta$  at  $10^{-4}$  M ionic strength based on the random sequential adsorption blocking function. The experiments shown with solid symbols were predicted using the same model parameters.

adjustable parameters when using either the LA or the RSA blocking models. The better performance of the RSA model suggests that it captures the essence of the deposition mechanisms observed in the experiments more closely than the LA model. Thus, the theoretical approach presented here seems to quantitatively explain the main features of colloid transport and deposition phenomena observed in granular porous media and might as well be used for prediction of the colloid breakthrough behavior with changes in physico-chemical conditions.

### ACKNOWLEDGMENTS

Financial support of this work by the Swiss Federal Institute of Technology and the U.S. National Science Foundation (Research Grant BES-9996240) is gratefully acknowledged.

### REFERENCES

- O'Melia, C. R., *Environ. Sci. Technol.* **14**, 1052 (1980).
- McDowell-Boyer, L. M., Hunt, J. R., and Sitar, N., *Water Resour. Res.* **22**, 1901 (1986).
- Kretzschmar, R., Borkovec, M., Grolimund, D., and Elimelech, M., *Adv. Agronomy* **66**, 121 (1999).
- Elimelech, M., Gregory, J., Jia, X., and Williams, R. A., "Particle Deposition and Aggregation. Measurement, Modelling, and Simulation." Butterworth-Heinemann, Stoneham, MA, 1995.
- Elimelech, M., and O'Melia, C. R., *Environ. Sci. Technol.* **24**, 1528 (1990).
- Elimelech, M., and O'Melia, C. R., *Langmuir* **6**, 1153 (1990).
- Ryde, N. P., and Matijevic, E., *Colloids Surf. A* **165**, 59 (2000).
- Matijevic, E., and Ryde, N. P., *J. Adhesion* **51**, 1 (1995).
- Grolimund, D., Elimelech, M., Borkovec, M., Barmettler, K., Kretzschmar, R., and Sticher, H., *Environ. Sci. Technol.* **32**, 3562 (1998).
- Kretzschmar, R., and Sticher, H., *Environ. Sci. Technol.* **31**, 3497 (1997).
- McDowell-Boyer, L. M., *Environ. Sci. Technol.* **26**, 586 (1992).
- Kretzschmar, R., Robarge, W. P., and Amoozegar, A., *Water Resour. Res.* **31**, 435 (1995).
- Yao, K. M., Habibian, M. T., and O'Melia, C. R., *Environ. Sci. Technol.* **5**, 1105 (1971).
- Rajagopalan, R., and Tien, C., *AICHE J.* **22**, 523 (1976).
- Elimelech, M., *J. Colloid Interface Sci.* **146**, 337 (1991).
- Litton, G. M., and Olson, T. M., *Environ. Sci. Technol.* **27**, 185 (1993).
- Litton, G. M., and Olson, T. M., *J. Colloid Interface Sci.* **165**, 522 (1994).
- Johnson, P. R., and Elimelech, M., *Langmuir* **11**, 801 (1995).
- Liu, D., Johnson, P. R., and Elimelech, M., *Environ. Sci. Technol.* **29**, 2963 (1995).
- Song, L., and Elimelech, M., *Colloids Surf. A* **73**, 49 (1993).
- Privman, V., Frisch, H. L., Ryde, N., and Matijevic, E., *J. Chem. Soc. Faraday Trans.* **87**, 1371 (1991).
- Ryde, N., Kihira, H., and Matijevic, E., *J. Colloid Interface Sci.* **151**, 421 (1992).
- Adamczyk, Z., Siwek, B., Zembela, M., and Belouschek, P., *Adv. Colloid Interface Sci.* **48**, 151 (1994).
- Ryde, N., Kallay, N., and Matijevic, E., *J. Chem. Soc. Faraday Trans.* **87**, 1377 (1991).
- Liang, L., McCarthy, J. F., Jolley, L. W., McNabb, J. A., and Mehlhorn, T. L., *Geochim. Cosmochim. Acta* **57**, 1987 (1993).
- Ryan, J. N., and Gschwend, P. M., *Environ. Sci. Technol.* **28**, 1717 (1994).
- Puls, R. W., and Powell, R. M., *Environ. Sci. Technol.* **26**, 614 (1992).
- Sugimoto, T., and Sakata, K., *J. Colloid Interface Sci.* **152**, 587 (1992).
- Schudel, M., Behrens, H., Holthoff, H., Kretzschmar, R., and Borkovec, M., *J. Colloid Interface Sci.* **196**, 241 (1997).
- Gregg, S. J., and Sing, K. S. W., "Adsorption, Surface Area and Porosity." Academic Press, London, 1982.
- Yoon, R. H., Salman, T., and Donnay, G., *J. Colloid Interface Sci.* **70**, 483 (1979).
- Villiermaux, J., in "Percolation Processes" (A. E. Rodrigues and D. Tondeur, Eds.), p. 83. Sijthoff, Amsterdam, 1981.
- Johnson, P. R., Sun, N., and Elimelech, M., *Environ. Sci. Technol.* **30**, 3284 (1996).
- Brenan, K. E., Campbell, S. L., and Petzold, L. R., "Numerical Solution of Initial-Value Problems in Differential-Algebraic Equations," Elsevier, Amsterdam, 1989.
- Petzold, L. R. "A description of DASSL: A differential/algebraic system solver." SAND82-8637, Sandia National Laboratories, Albuquerque, NM, 1982.
- Semmler, M., Mann, E. K., Ricka, J., and Borkovec, M., *Langmuir* **14**, 5127 (1998).
- More, J., Garbow, B., and Hillstrom, K. "User guide for MINPACK-1," Rep. No. ANL-80-74, Argonne National Labs Report, Argonne, Illinois, 1980.
- Warzynski, P., *Adv. Colloid Interface Sci.* **84**, 47 (2000).